Cell Reports
Report

Structure of Human cGAS Reveals a Conserved Family of Second-Messenger Enzymes in Innate Immunity

Philip J. Kranzusch,[1,2] Amy Si-Ying Lee,[1,2] James M. Berger,[1,5,*] and Jennifer A. Doudna[1,2,3,4,5,*]
[1]Department of Molecular & Cell Biology
[2]Center for RNA Systems Biology
[3]Department of Chemistry
[4]Howard Hughes Medical Institute (HHMI)
University of California, Berkeley, CA 94720, USA
[5]Physical Biosciences Division, Lawrence Berkeley National Laboratory, Berkeley, CA 94720, USA
*Correspondence: jmberger@berkeley.edu (J.M.B.), doudna@berkeley.edu (J.A.D.)
http://dx.doi.org/10.1016/j.celrep.2013.05.008

SUMMARY

Innate immune recognition of foreign nucleic acids induces protective interferon responses. Detection of cytosolic DNA triggers downstream immune signaling through activation of cyclic GMP-AMP synthase (cGAS). We report here the crystal structure of human cGAS, revealing an unanticipated zinc-ribbon DNA-binding domain appended to a core enzymatic nucleotidyltransferase scaffold. The catalytic core of cGAS is structurally homologous to the RNA-sensing enzyme, 2′-5′ oligo-adenylate synthase (OAS), and divergent C-terminal domains account for specific ligand-activation requirements of each enzyme. We show that the cGAS zinc ribbon is essential for STING-dependent induction of the interferon response and that conserved amino acids displayed within the intervening loops are required for efficient cytosolic DNA recognition. These results demonstrate that cGAS and OAS define a family of innate immunity sensors and that structural divergence from a core nucleotidyltransferase enables second-messenger responses to distinct foreign nucleic acids.

INTRODUCTION

The human innate immune system deploys cellular sensors to detect and respond to the presence of pathogens. Many of these sensors activate innate immunity by recognizing aberrant nucleic acid localization within the cell (Holm et al., 2013; Kagan, 2012; Medzhitov, 2007). Foreign RNA detection by toll-like receptors and RIG-I has been studied in some detail, but the mechanistic basis of DNA detection and signal initiation within the cytoplasm has remained enigmatic. Recently, the enzyme cyclic GMP-AMP synthase (cGAS) was identified as requisite for DNA detection, and cyclic GMP-AMP (cGAMP) was shown to function as a second messenger that stimulates innate immunity through the endoplasmic reticulum receptor STING (Sun et al., 2013; Wu et al., 2013). The identification of cGAS explains the potent immune response to cytosolic DNA and reveals a major source of ligands responsible for STING activation, but it does not show how cGAS responds selectively to DNA and how it relates to other nucleic acid receptors.

RESULTS AND DISCUSSION

To investigate the mechanism and evolution of cytosolic DNA recognition, we determined the 2.5 Å crystal structure of human cGAS. Analysis of purified human cGAS by partial proteolytic digestion revealed a protease-sensitive ~150-amino-acid-long N terminus attached to a protease-resistant fragment containing all regions previously determined to be required for cytosolic DNA detection (Figure S1) (Sun et al., 2013). A fluorescence scan of crystallized cGAS (amino acids 157–522) detected zinc, and a single bound zinc ion provided anomalous X-ray diffraction data sufficient for initial phase determination (Table S1 and Figure S2). Human cGAS adopts the overall fold of other template-independent nucleotidyltransferase (NTase) enzymes, including transfer RNA (tRNA) NTases (CCA-adding enzymes) and the RNA sensor 2′-5′ oligo-adenylate synthase (OAS) (Donovan et al., 2013; Hartmann et al., 2003; Xiong and Steitz, 2004). Appended to the NTase core scaffold is an unanticipated zinc-ribbon domain resulting from a unique sequence insertion conserved in the C-terminal domain (C domain) of all vertebrate cGAS enzymes (Figures 1A, 1B, and S3).

The structure of cGAS reveals an evolutionary link with the human double-stranded RNA (dsRNA) sensor OAS. Upon recognition of cytosolic dsRNA, OAS produces the second messenger 2′-5′ oligo-adenylate (Hovanessian et al., 1977; Kerr and Brown, 1978), which triggers innate immunity by activating RNase L and translation arrest (Baglioni et al., 1978; Hovanessian et al., 1979). In line with their roles as cytoplasmic sensors that signal the presence of foreign RNA and DNA through the production of second-messenger nucleic acids, OAS and cGAS contain an NTase core domain that is structurally conserved (Figure 1C). In contrast to the catalytic domain, the more divergent C domain is rotated in cGAS with respect to its orientation in the OAS structure, consistent with altered geometry enabling cGAS to accommodate dsDNA.

Adjacent to the conserved enzymatic scaffold of cGAS and OAS is a positively charged cleft at the interface between the

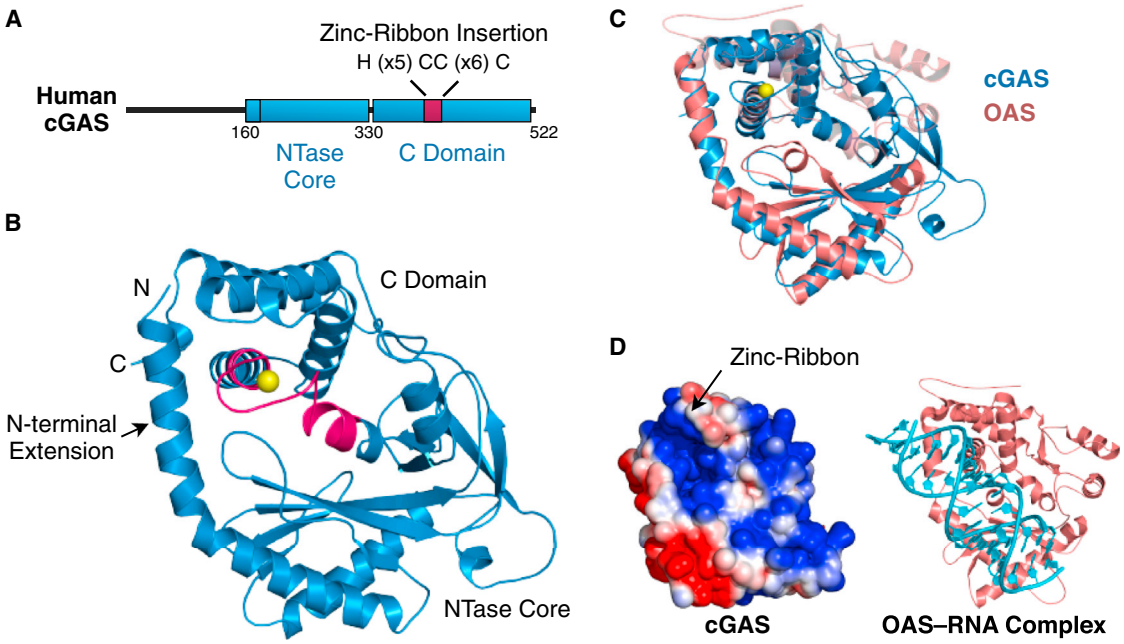

Figure 1. Structure of Human cGAS

(A) Cartoon schematic of the human cGAS primary sequence.

(B) Overall structure of human cGAS, with the N-terminal helical extension, NTase core scaffold, and C-terminal domain (C domain) shown in blue. A unique zinc-ribbon insertion is shown in magenta, and the zinc ion is shown in yellow.

(C) Structural overlay of cytosolic nucleic acid sensors, human cGAS (blue), and human OAS (pink).

(D) Electrostatic surface potential of cGAS (left); a conserved, positively charged nucleic-acid-binding cleft equivalent to the OAS dsRNA-binding site, as observed in the structure of an OAS-dsRNA complex (right; PDB code 4IG8).

See also Figures S2 and S3.

N-terminal extension and the C domain alpha-helical lobe (Figures 1C and 1D). When compared to the crystal structure of dsRNA-bound OAS (Donovan et al., 2013), the location of the positively charged cleft in cGAS suggests that OAS and cGAS most likely use a similar binding surface to engage double-stranded nucleic acid ligands (Figure 1D). Insertion of the H(X_5)CC(X_6)C zinc-ribbon binding motif between residues 389 and 405 induces structural rearrangement of the cGAS C domain, relative to OAS. The zinc-coordination site buttresses a charged loop that alters the geometry of the positive binding cleft, consistent with the differing nucleic-acid-binding specificities of cGAS and OAS enzymes, as discussed below.

Previous studies, which relied on detection of cGAMP by mass spectrometry or indirect immune-stimulation assays requiring cellular extracts (Sun et al., 2013), did not analyze cGAS product species and activating conditions directly. Using purified components, we reconstituted DNA-dependent cyclic dinucleotide production by cGAS and analyzed the products using thin layer chromatography. Minimal cGAS activity requires GTP, ATP, and an activating dsDNA ligand (Figure 2A). cGAS dinucleotide synthesis activity is abolished by E225A and D227A mutations to the active site (Figure 2A, "Mut"), confirming the specificity of our in vitro reconstitution system. Surprisingly, the cGAS GMP–AMP dinucleotide product migrates differently from chemically synthesized 3′-5′ linked cGAMP (Figure 2B and Figure S4A). Concurrent experiments revealed that the cGAS product is a hybrid cyclic nucleotide containing a noncanonical 2′-5′ glycosidic linkage (Diner et al., 2013).

We observed robust cGAS catalytic activity only in the presence of dsDNA (Figure 2C). While single-stranded DNA (ssDNA) substrates weakly stimulate catalysis, we detected no dinucleotide synthesis in the presence of ssRNA or dsRNA ligands or in the absence of nucleic acids (Figure 2C). Strict DNA-stimulated activity was not observed for murine cGAS (Sun et al., 2013), suggesting that the human variant has evolved more stringent ligand-activation requirements. The construct used for structural studies, lacking the poorly conserved ~150-amino-acid-long N terminus, retains enzymatic activity and DNA selectivity, indicating that all domains required for dsDNA detection and immune signaling are present in our crystal structure (Figure S4B). Fluorescence anisotropy experiments confirmed that cGAS specifically engages dsDNA (K_d ~87.6 nM), whereas Mab21L2, an NTase lacking the zinc-ribbon domain insertion, cannot interact as robustly with DNA substrates (Figure 2D). cGAS had a dramatically reduced affinity for ssDNA (K_d ~1.5 μM), consistent with the limited ability of single-stranded nucleic acids to stimulate enzymatic activity (Figure 2D). The affinity of cGAS for dsDNA decreases for dsDNA ligands shorter than two helical turns (Figure S4C). This finding is consistent with previous results demonstrating that at least 20–30 base pairs (bp) of dsDNA are required for efficient stimulation of innate immunity (Ablasser et al., 2009; Karayel et al., 2009; Stetson and Medzhitov, 2006).

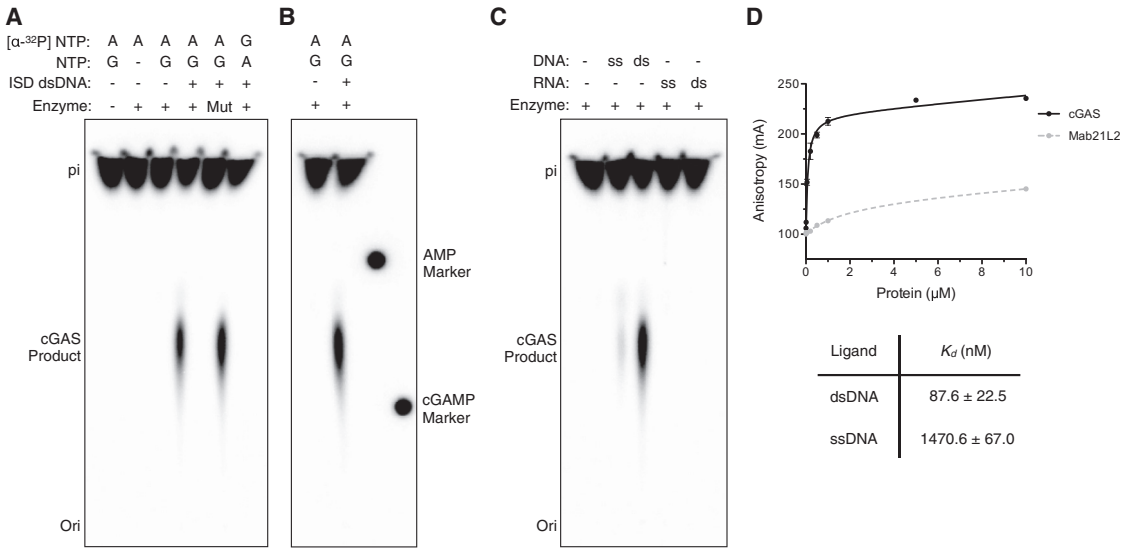

Figure 2. In Vitro Reconstitution of cGAS Dinucleotide Signaling

(A and B) Thin-layer chromatography analysis of cGAS cyclic dinucleotide synthesis. Purified full-length cGAS was incubated with substrate nucleotides and interferon stimulatory DNA (ISD) as indicated. Prior to analysis, reactions were terminated by treatment with alkaline phosphatase to remove free nucleotide triphosphate. An E225A/D227A mutation to the cGAS active site (Mut) ablates cyclic dinucleotide production. Dotted radioactive spots corresponding to UV-shadowed AMP and 3′-5′ linked cGAMP markers demonstrate that the product of cGAS activity is a noncanonical dinucleotide product.

(C) cGAS activity is strictly dependent on dsDNA activation.

(D) Fluorescence anisotropy analysis of cGAS binding to dsDNA. Error bars represent the SD from the mean of at least three independent experiments.

See also Figure S4.

The zinc-ribbon structural domain is conserved among vertebrate cGAS members, but it is not found in other OAS and related NTase family members (Figure 3A). Zinc coordination in cGAS occurs by an atypical $H(X_5)CC(X_6)C$ motif that most closely resembles HCCC-type zinc ribbons found in TAZ domains (Laity et al., 2001). In the human cGAS structure, the first pair of

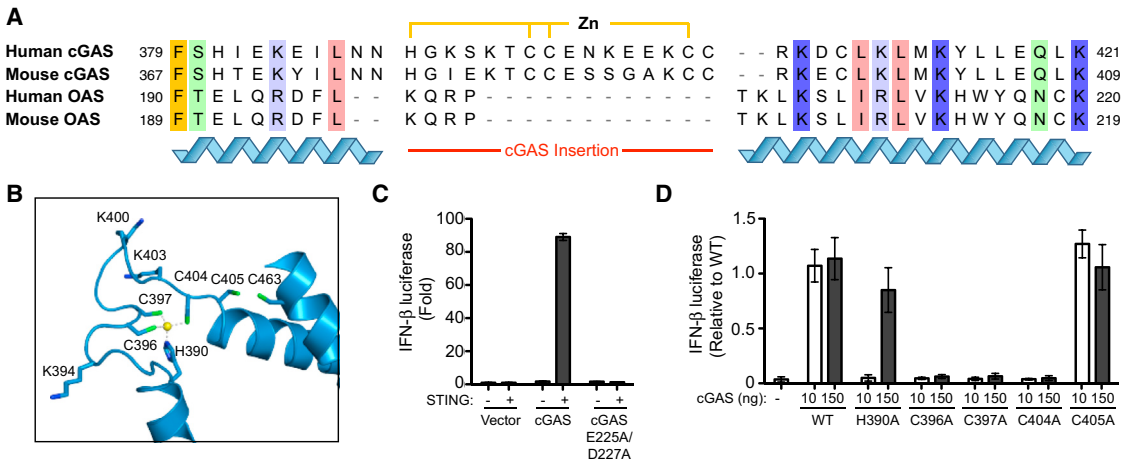

Figure 3. cGAS Zinc-Ribbon Domain Is Essential for Interferon Signaling

(A) Sequence alignment of human and murine cGAS and OAS cytosolic sensors. The unique cGAS zinc-ribbon insertion domain and coordinating residues are indicated.

(B) Structural details of the zinc-coordination site. Highly conserved amino acids are labeled.

(C) Reconstitution of STING-dependent cGAS signaling in cells. Luciferase production under control of the interferon-β (IFN-β) promoter demonstrates that DNA-stimulated cGAS signaling only activates the IFN pathway in the presence of STING; cGAS E225A/D227A contains two point mutations in the enzymatic active site.

(D) Mutational analysis of the cGAS zinc-ribbon motif. Substitutions to the zinc-coordination motif (H390A, C396A, C397A, C404A) abolish cGAS activity when expressed at low levels (10 ng), and overexpression demonstrates that only H390A retains weakened signaling potential (150 ng).

In (C) and (D), error bars represent the SD from the mean of at least three independent experiments.

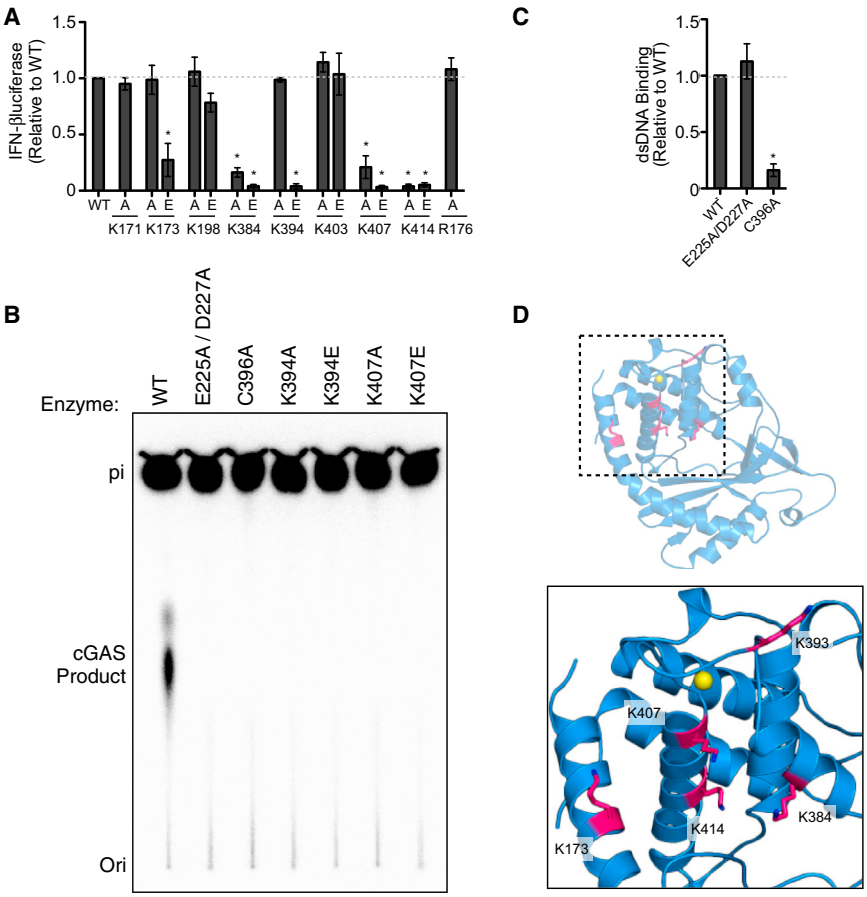

Figure 4. cGAS Zinc Ribbon and Positive DNA-Binding Cleft Are Essential for DNA Recognition and Catalytic Activity

(A) Reconstitution of STING-dependent cGAS signaling in cells as described in Figure 3. Single alanine and glutamine mutations to conserved positively charged amino acids within the DNA-binding cleft demonstrate that K173, K384, K407, and K414 are required for efficient cytosolic DNA detection.

(B) In vitro reconstitution of cGAS dinucleotide synthesis using purified components as described in Figure 2 (*$p < 0.001$). Mutations to the active site (E225A/D227A), zinc-coordination motif (C396A) and conserved DNA-binding cleft (K394A, K394E, K407A, K407E) all abolish DNA-stimulated enzymatic activity.

(C) The ability of mutant cGAS enzymes to engage a 45 bp double-stranded ISD substrate was measured by fluorescence polarization with the use of 2 μM of purified protein as described in Figure 2D (*$p < 0.001$). Mutations to the active site (E225A/D227A) do not disrupt DNA interactions, whereas disruption of the zinc-coordination motif drastically inhibits the ability of cGAS to interact with dsDNA.

(D) Structural details of the DNA-binding cleft formed by the N-terminal extension and zinc-ribbon domain. Conserved positively charged amino acids identified as critical for DNA-stimulated activity are labeled and shown in magenta. In (A) and (C), error bars represent the SD from the mean of at least three independent experiments. See also Figure S1C.

adjacent cysteine residues (C396 and C397) each coordinate the zinc ion. In the second cysteine pair, C404 completes the coordination, and neighboring C405 flips out to form a paired cysteine interaction with downstream C463 from alpha helix 11 (Figures 3A and 3B).

To examine the role of zinc ion coordination and to extend our biochemical studies to cellular interferon (IFN) signaling in the context of the endoplasmic reticulum adaptor protein STING (Burdette and Vance, 2013; Ishikawa and Barber, 2008; Sun et al., 2009; Zhong et al., 2008), we tested the function of site-specific cGAS protein mutations in a cell-based assay. Using an IFN-β-stimulated promoter cassette upstream of firefly luciferase, we first confirmed that intracellular cGAS signaling requires the presence of STING to confer second-messenger detection (Figure 3C). As expected, a double mutation to the cGAS active site (E225A/D227A) that prevents cyclic dinucleotide synthesis abolished IFN signaling (Figure 3C). Mutations at each position in the zinc-coordination site near the DNA-binding cleft also ablated or severely impaired detectable IFN-response activation (Figure 3D), confirming that this motif is essential for innate immune signaling; however, a C405A mutation did not inhibit IFN signaling, indicating that the paired cysteine interaction with alpha helix 11 is not critical for cytosolic DNA recognition (Figure 3D).

We also examined conserved positively charged positions along the potential DNA-binding cleft (Figure S3). Single alanine or glutamate substitutions along the N-terminal alpha helical extension and within the conserved zinc-ribbon loop dramatically reduced the ability of cGAS to detect cytosolic DNA, demonstrating the importance of conserved residues in this region of the protein (Figure 4A). Biochemical analysis with purified human cGAS confirmed that mutations to the active site, zinc-coordination motif, and conserved charged cleft ablate DNA-stimulated dinucleotide synthesis activity (Figure 4B). Whereas active-site mutants retained affinity for dsDNA, a C396A mutation disrupting the zinc-coordination motif prevented dsDNA interactions (Figure 4C). These data show that dsDNA engagement is critical for activation of the enzymatic potential of cGAS and that conserved, positively charged amino acids along with the unique zinc-ribbon insertion are essential for DNA recognition (Figure 4D). We note that the presence of the unstructured N-terminal tail greatly enhanced the stability of cGAS protein during purification (data not shown), hinting that the N terminus may play a further role in stabilization or autoinhibition, as observed with other innate immune cellular receptors (Sun et al., 2013).

Concurrent with our structural analysis of the human cGAS enzyme, Patel and colleagues determined the structure of murine cGAS bound to dsDNA and product dinucleotide (Gao et al., 2013). The overall sequence identity of human and murine cGAS is ~55% (Figure S3), and structures of both enzymes now

reveal that rapid mammalian evolution has occurred in patches along the surface of the enzyme, indicative of positive selection and host–pathogen conflict (Daugherty and Malik, 2012). The critical role of cGAS in innate immunity and cytosolic DNA detection (Sun et al., 2013) suggests that the mechanisms by which intracellular dsDNA pathogens subvert cGAS-dependent DNA recognition may aid in detecting the regulation of cGAS enzymatic activity and cytosolic signaling.

The recent discovery of cGAS as a cytosolic DNA sensor is an important advance in the field of innate immunity (Sun et al., 2013), and the structure described here presents essential molecular details of cGAS biochemistry. The structure of human cGAS, revealing the similar folds of cGAS and OAS, implicates a common evolutionary ancestor as the origin of a family of structurally related but functionally distinct cytosolic nucleic acid sensors. Although multiple duplications of the *OAS* genes had been considered to be an outlier grouping of restriction factors, it is now clear that the OAS/cGAS NTase scaffold has evolved as part of a second-messenger system to rapidly generate and amplify di- and oligonucleotide signals upon pathogen recognition. cGAS and OAS constitute a family of catalytic OAS-like second-messenger receptors (OLRs), which together with Toll-like receptors (TLRs) and RIG-I-like receptors (RLRs) form the front line of immune defense against foreign pathogens.

EXPERIMENTAL PROCEDURES

Protein Purification

Full-length human *cGAS* and *cGAS* truncations were subjected to PCR amplification from a previously described IFN-stimulated gene cDNA library (kind gift from J. Schoggins and C. Rice, Rockefeller University; Schoggins et al., 2011) and cloned into a custom pET vector optimized for *E. coli* expression of an N-terminal 6×His-MBP-TEV fusion protein (Kranzusch and Whelan, 2011). Proteins were overexpressed at 16°C in BL21-RIL DE3 *E. coli* (along with pRARE2 human tRNA plasmid) (Agilent) grown in 2×YT media for 20 hr after induction with 0.5 M IPTG. Recombinant protein was purified by successive Ni-NTA affinity, Heparin ion exchange, and Superdex 75 chromatography steps. Cells were lysed by sonication in 20 mM HEPES (pH 7.5), 400 mM NaCl, 10% glycerol, 30 mM imidazole, 1 mM PMSF (supplemented with Complete Protease Inhibitor, Roche), and 1 mM TCEP. Clarified lysate was bound to Ni-NTA agarose (QIAGEN), and resin was washed with lysis buffer supplemented to 1 M NaCl prior to the elution of bound protein using lysis buffer supplemented to 300 mM imidazole. MBP-tagged proteins were concentrated to ~30–40 mg ml^{-1} and digested with Tobacco Etch Virus protease for ~16 hr at 4°C. cGAS was separated from MBP on a 5 ml Heparin HiTrap column (GE Life Sciences) with the use of a linear gradient of 250–1000 mM NaCl. Proteins were further purified by size-exclusion chromatography on a Superdex 75 16/60 column in 20 mM HEPES (pH 7.5), 150 mM KCl, and 1 mM TCEP. Eluted protein was concentrated to ~10–20 mg ml^{-1} and used immediately in crystallography experiments or flash-frozen in the presence of 10% glycerol in liquid nitrogen and stored at −80°C for biochemical experiments.

Mutant cGAS variants were purified as described for the wild-type human enzyme, except instead of TEV digestion, MBP-tagged proteins were dialyzed overnight at 4°C against buffer containing 20 mM HEPES (pH 7.5), 150 mM KCl, 10% glycerol, and 1 mM TCEP. Wild-type and mutant MBP-tagged cGAS enzymes were concentrated to ~10–12 mg ml^{-1}, flash-frozen in liquid nitrogen, and stored at −80°C for biochemical experiments.

Crystallization and Structure Determination

Full-length cGAS protein was digested with increasing amounts of trypsin at 25°C for 30 min to allow the identification of stable constructs for crystallography trials. Trypsin reactions were terminated by the addition of 1 mM PMSF for SDS-PAGE analysis or an equal volume of 6 M guanidine hydrochloride for mass spectrometry. A human cGAS 157–522 amino acid construct was designed on the basis of mass spectrometry results and phylogenetic alignment, and the cGAS truncation was purified as described above. Initial crystals of cGAS amino acids 157–522 were obtained at 18°C in 1:1 hanging drops set with 10 mg ml^{-1} protein and 50 mM KCl, 10 mM $MgCl_2$, and 15% PEG-6000 well solution after 36 hr of growth, then optimized in 15-well hanging drop trays (QIAGEN) with the use of 1.5:0.5 drops with 8 mg ml^{-1} protein and 44 mM KCl, 10 mM $MgCl_2$, 25 mM Tris (pH 7.0), 15 mM Tris (pH 9.0), and 6.9% PEG-6000. Crystals were harvested with nylon loops and cryoprotected by incubation in well solution supplemented to 25% ethylene glycol for 30–60 s prior to being flash-frozen in liquid nitrogen. Initial native X-ray data were measured under cryogenic conditions at the Lawrence Berkeley National Laboratory Advanced Light Source (Beamline 8.3.1), and zinc anomalous data were measured at the Stanford Synchrotron Radiation Lightsource (Beamlines 11.1 and 12.2). Selenium-substituted cGAS amino acids 157–522 were purified under identical conditions, and crystals of this sample grew in 44 mM KCl, 10 mM $MgCl_2$, 25 mM Tris (pH 7.0), 15 mM Tris (pH 9.0), and 9.7% PEG-6000. These crystals were optimized through microseeding and streak seeding of crushed native crystals with the use of a Kozak whisker. X-ray diffraction data from selenium-containing crystals were measured at the Stanford Synchrotron Radiation Lightsource (Beamline 12.2).

X-ray diffraction data were processed with XDS and SCALA (Kabsch, 2010). Indexed crystals belonged to the orthorhombic spacegroup $P2_12_12$ with one copy of cGAS in the asymmetric unit. The zinc site was identified with HySS within PHENIX (Adams et al., 2010), and SOLVE/RESOLVE was used in calculating an initial map (Terwilliger, 1999). After initial model building in Coot (Emsley and Cowtan, 2004), iterative rounds of model building and refinement were conducted with PHENIX until all interpretable electron density was modeled. With the use of anomalous scattering data from selenium atoms, the five selenium sites were located by molecular-replacement phasing and used for verification of the register and position of the cGAS model.

In Vitro Reconstitution of cGAS Cyclic Dinucleotide Synthesis

DNA-dependent human cGAS cyclic dinucleotide synthesis was reconstituted with the use of recombinant full-length cGAS and a 45 bp double-stranded interferon stimulatory DNA (ISD) (Integrated DNA Technologies) (Stetson and Medzhitov, 2006). cGAS (final concentration ~2 μM) or equal volumes of gel-filtration buffer were incubated with double-stranded ISD (final concentration ~2 μM) in the presence of 25 μM ATP and GTP and [α-^{32}P] ATP or GTP (~10 μCi) as indicated. All reactions included 50 mM KCl, 5 mM $Mg(OAc)_2$, 50 mM Tris (pH 7.0), 1 mM TCEP, and 0.1 mg ml^{-1} BSA (NEB), and reactions were incubated at 37°C for 1.5 hr. Reactions were terminated with the addition of 5 U of alkaline phosphatase (New England Biolabs) and incubation at 37°C for 30 min. One microliter of each reaction was spotted onto a PEI-Cellulose F thin-layer chromatography plate (EMD Biosciences), and reaction products were separated with the use of 1.5 M KH_2PO_4 (pH 3.8) as solvent. Plates were dried at 80°C for 30 min, and radiolabeled products were detected with a phosphor screen and the Storm phosphorimager (GE Life Sciences). Where indicated, controls consisting of chemically synthesized AMP (Jena Biosciences) or 3′-5′ linked cGAMP (a kind gift from S. Wilson and M. Hammond, University of California, Berkeley) were imaged with a ~254 nm light for UV shadowing and marked by the spotting of a dot of radiolabeled ATP prior to phosphor-screen exposure. Alternatively, reactions were carried out in the presence of 45 bp of single-stranded ISD (sequence: 5′-TACAG ATCTACTAGTGATCTATGACTGATCTGTACATGATCTACA-3′) (Stetson and Medzhitov, 2006) or ssRNA and dsRNA formed by the annealing of two chemically synthesized RNA oligomers (sequence: 5′-CGGUAGAGCUCACAU GAUGG-3′) (Integrated DNA Technologies).

Fluorescence anisotropy DNA-interaction studies were carried out with the use of 5′ fluorescein-derived DNA oligomers with the ISD DNA sequence and indicated sizes (Integrated DNA Technologies). With the use of the same buffer conditions used during cyclic dinucleotide synthesis reactions, cGAS was incubated with DNA for 30 min at 25°C prior to fluorescence polarization measurements obtained with a fluorimeter (Perkin Elmer). Polarization data were converted to anisotropy, and data from independent experiments were combined and analyzed with GraphPad Prism software for the determination of binding constants.

Cell-Based IFN-β Luciferase Assay

293T cells were plated into tissue-culture-treated 96-well plates for transfection. Cells were transfected as indicated (Figures 3C, 3D, 4A, and 4C), along with IFN-β firefly luciferase (a kind gift from J.U. Jung, University of Southern California, Los Angeles) and TK-Renilla luciferase reporter plasmids. At 24 hr after transfection, cells were lysed in passive lysis buffer (Promega) for 15 min. Luminescence was measured on a Veritas Microplate Luminometer (Turner Biosystems) with the use of Dual-Luciferase Reporter Assay System according to the manufacturer's instructions (Promega). The relative IFN-β expression was calculated by normalizing firefly luciferase to Renilla luciferase activity. Mutations in cGAS were generated by site-directed mutagenesis through the use of the QuikChange methodology (Stratagene). As indicated (Figures 4A and 4C), statistical significance was calculated with an unpaired, two-tailed t test.

ACCESSION NUMBERS

Coordinates of human cGAS have been deposited in the RCSB Protein Data Bank under accession number 4KM5.

SUPPLEMENTAL INFORMATION

Supplemental Information includes four figures and one table and can be found with this article online at http://dx.doi.org/10.1016/j.celrep.2013.05.008.

LICENSING INFORMATION

ACKNOWLEDGMENTS

Experiments were designed by P.J.K. in consultation with J.M.B. and J.A.D., structural and biochemical work was performed by P.J.K., and cell-signaling assays were performed by A.S.Y.L. The manuscript was written by P.J.K. and J.A.D., and all authors contributed to editing the manuscript and support the conclusions. The authors are grateful to the staff at Beamlines 11.1 and 12.2 of the Stanford Synchrotron Radiation Lightsource (SSRL) and Beamline 8.3.1 of the Lawrence Berkeley National Lab Advanced Light Source for their technical assistance; T. Doukov (Stanford, SSRL) for assistance with data collection and analysis; M. Jinek (University of Zurich), A. Lyubimov, and J. Cate (University of California, Berkeley) for advice on phase determination and model building; D. King (HHMI, University of California, Berkeley) for mass spectrometry; J. Schoggins and C. Rice (Rockefeller University) for reagents; M. Solovykh for technical assistance; and Y. Bai, S. Floor, and members of the Doudna and Berger labs for helpful comments and discussion. This work was funded by HHMI (J.A.D.), the G. Harold and Leila Y. Mathers Foundation (J.M.B.), and the NIGMS Center for RNA Systems Biology (P.J.K., A.S.Y.L., and J.A.D.). J.A.D. is an HHMI Investigator.

Received: May 5, 2013
Accepted: May 9, 2013
Published: May 23, 2013

REFERENCES

Ablasser, A., Bauernfeind, F., Hartmann, G., Latz, E., Fitzgerald, K.A., and Hornung, V. (2009). RIG-I-dependent sensing of poly(dA:dT) through the induction of an RNA polymerase III-transcribed RNA intermediate. Nat. Immunol. *10*, 1065–1072.

Adams, P.D., Afonine, P.V., Bunkóczi, G., Chen, V.B., Davis, I.W., Echols, N., Headd, J.J., Hung, L.W., Kapral, G.J., Grosse-Kunstleve, R.W., et al. (2010). PHENIX: a comprehensive Python-based system for macromolecular structure solution. Acta Crystallogr. D Biol. Crystallogr. *66*, 213–221.

Baglioni, C., Minks, M.A., and Maroney, P.A. (1978). Interferon action may be mediated by activation of a nuclease by pppA2'p5'A2'p5'A. Nature *273*, 684–687.

Burdette, D.L., and Vance, R.E. (2013). STING and the innate immune response to nucleic acids in the cytosol. Nat. Immunol. *14*, 19–26.

Daugherty, M.D., and Malik, H.S. (2012). Rules of engagement: molecular insights from host-virus arms races. Annu. Rev. Genet. *46*, 677–700.

Diner, E.J., Burdette, D.L., Monroe, K.M., Wilson, S.C., Canlas, C., Lemmens, E.E., Lauer, P., Dubensky, T.W., Hammon, M.C., and Vance, R.E. (2013). The innate immune DNA sensor cGAS produces a noncanonical cyclic dinucleotide that activates human STING. Cell Rep. Published online May 23, 2013. http://dx.doi.org/10.1016/j.celrep.2013.05.009.

Donovan, J., Dufner, M., and Korennykh, A. (2013). Structural basis for cytosolic double-stranded RNA surveillance by human oligoadenylate synthetase 1. Proc. Natl. Acad. Sci. USA *110*, 1652–1657.

Emsley, P., and Cowtan, K. (2004). Coot: model-building tools for molecular graphics. Acta Crystallogr. D Biol. Crystallogr. *60*, 2126–2132.

Gao, P., Ascano, M., Wu, Y., Barchet, W., Gaffney, B.L., Zillinger, T., Serganov, A.A., Liu, Y., Jones, R.A., Hartmann, G., et al. (2013). Cyclic [G(2′,5′)pA(3′,5′)p] Is the Metazoan Second Messenger Produced by DNA-Activated Cyclic GMP-AMP Synthase. Cell. Published online May 3, 2013. http://dx.doi.org/10.1016/j.cell.2013.04.046.

Hartmann, R., Justesen, J., Sarkar, S.N., Sen, G.C., and Yee, V.C. (2003). Crystal structure of the 2′-specific and double-stranded RNA-activated interferon-induced antiviral protein 2′-5′-oligoadenylate synthetase. Mol. Cell *12*, 1173–1185.

Holm, C.K., Paludan, S.R., and Fitzgerald, K.A. (2013). DNA recognition in immunity and disease. Curr. Opin. Immunol. *25*, 13–18.

Hovanessian, A.G., Brown, R.E., and Kerr, I.M. (1977). Synthesis of low molecular weight inhibitor of protein synthesis with enzyme from interferon-treated cells. Nature *268*, 537–540.

Hovanessian, A.G., Wood, J., Meurs, E., and Montagnier, L. (1979). Increased nuclease activity in cells treated with pppA2'p5'A2'p5′ A. Proc. Natl. Acad. Sci. USA *76*, 3261–3265.

Ishikawa, H., and Barber, G.N. (2008). STING is an endoplasmic reticulum adaptor that facilitates innate immune signalling. Nature *455*, 674–678.

Kabsch, W. (2010). Xds. Acta Crystallogr. D Biol. Crystallogr. *66*, 125–132.

Kagan, J.C. (2012). Signaling organelles of the innate immune system. Cell *151*, 1168–1178.

Karayel, E., Bürckstümmer, T., Bilban, M., Dürnberger, G., Weitzer, S., Martinez, J., and Superti-Furga, G. (2009). The TLR-independent DNA recognition pathway in murine macrophages: Ligand features and molecular signature. Eur. J. Immunol. *39*, 1929–1936.

Kerr, I.M., and Brown, R.E. (1978). pppA2'p5'A2'p5'A: an inhibitor of protein synthesis synthesized with an enzyme fraction from interferon-treated cells. Proc. Natl. Acad. Sci. USA *75*, 256–260.

Kranzusch, P.J., and Whelan, S.P. (2011). Arenavirus Z protein controls viral RNA synthesis by locking a polymerase-promoter complex. Proc. Natl. Acad. Sci. USA *108*, 19743–19748.

Laity, J.H., Lee, B.M., and Wright, P.E. (2001). Zinc finger proteins: new insights into structural and functional diversity. Curr. Opin. Struct. Biol. *11*, 39–46.

Medzhitov, R. (2007). Recognition of microorganisms and activation of the immune response. Nature *449*, 819–826.

Schoggins, J.W., Wilson, S.J., Panis, M., Murphy, M.Y., Jones, C.T., Bieniasz, P., and Rice, C.M. (2011). A diverse range of gene products are effectors of the type I interferon antiviral response. Nature *472*, 481–485.

Stetson, D.B., and Medzhitov, R. (2006). Recognition of cytosolic DNA activates an IRF3-dependent innate immune response. Immunity *24*, 93–103.

Sun, W., Li, Y., Chen, L., Chen, H., You, F., Zhou, X., Zhou, Y., Zhai, Z., Chen, D., and Jiang, Z. (2009). ERIS, an endoplasmic reticulum IFN stimulator, activates innate immune signaling through dimerization. Proc. Natl. Acad. Sci. USA *106*, 8653–8658.

Sun, L., Wu, J., Du, F., Chen, X., and Chen, Z.J. (2013). Cyclic GMP-AMP synthase is a cytosolic DNA sensor that activates the type I interferon pathway. Science *339*, 786–791.

Terwilliger, T.C. (1999). Reciprocal-space solvent flattening. Acta Crystallogr. D Biol. Crystallogr. *55*, 1863–1871.

Wu, J., Sun, L., Chen, X., Du, F., Shi, H., Chen, C., and Chen, Z.J. (2013). Cyclic GMP-AMP is an endogenous second messenger in innate immune signaling by cytosolic DNA. Science *339*, 826–830.

Xiong, Y., and Steitz, T.A. (2004). Mechanism of transfer RNA maturation by CCA-adding enzyme without using an oligonucleotide template. Nature *430*, 640–645.

Zhong, B., Yang, Y., Li, S., Wang, Y.Y., Li, Y., Diao, F., Lei, C., He, X., Zhang, L., Tien, P., and Shu, H.B. (2008). The adaptor protein MITA links virus-sensing receptors to IRF3 transcription factor activation. Immunity *29*, 538–550.

Cell PRESS
Open ACCESS

SUPPLEMENTAL REFERENCES

Katoh, K., and Standley, D.M. (2013). MAFFT multiple sequence alignment software version 7: improvements in performance and usability. Mol. Biol. Evol. *30*, 772–780.

Waterhouse, A.M., Procter, J.B., Martin, D.M., Clamp, M., and Barton, G.J. (2009). Jalview Version 2—a multiple sequence alignment editor and analysis workbench. Bioinformatics *25*, 1189–1191.

Cell PRESS
Open ACCESS

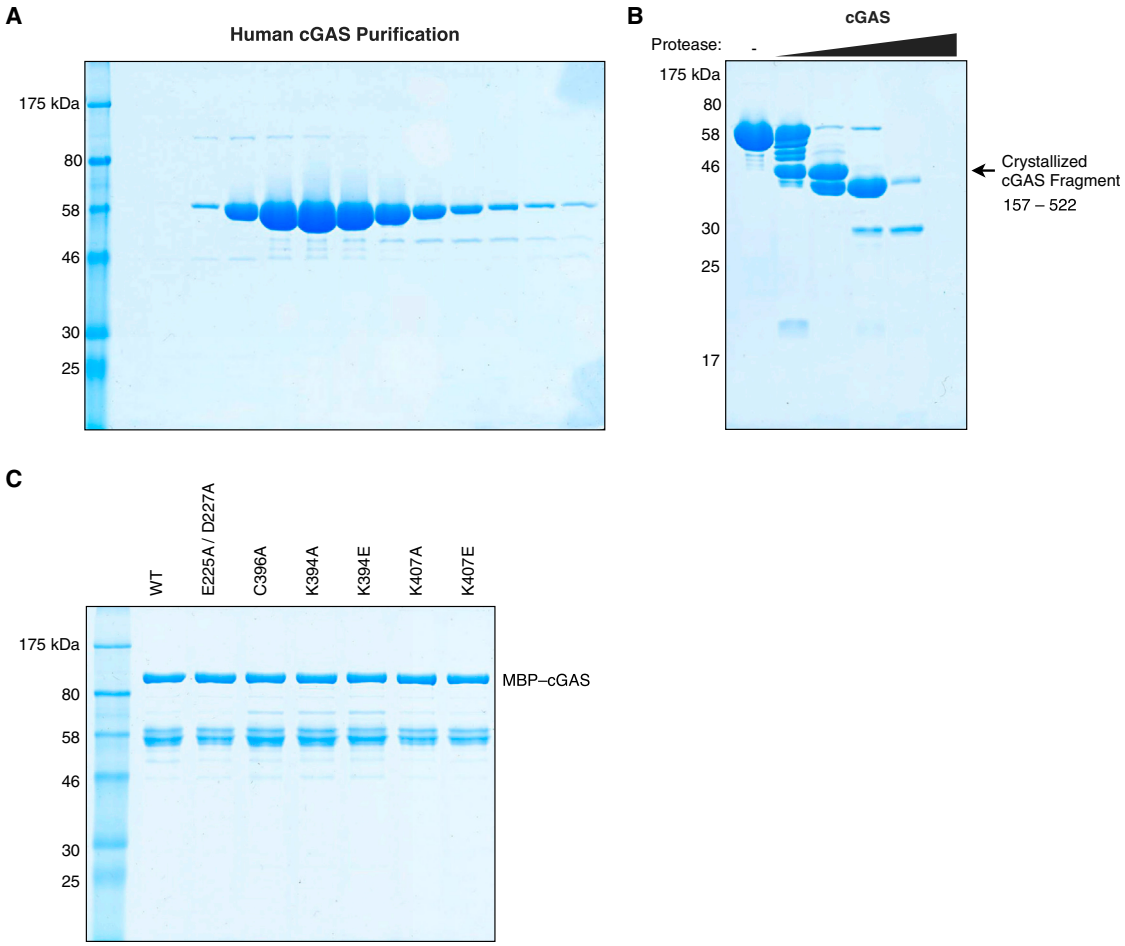

Figure S1. Purification and Proteolytic Digestion of Human cGAS, Related to Figures 1 and 4

(A) SDS-PAGE analysis of cGAS protein fractions following final size-exclusion chromatography purification step.

(B) Proteolytic digestion of full-length cGAS. Recombinant protein was treated with increasing concentrations of trypsin protease and analyzed by SDS-PAGE as described in methods.

(C) SDS-PAGE analysis of wild-type and mutant MBP-tagged cGAS variants. MBP-tagged cGAS-degradation products (~58 kDa species) copurify with full-length enzyme during first step purification, but these species do not impair enzymatic activity and are removed during subsequent purification steps for the wild-type protein used in biochemical and structural studies.

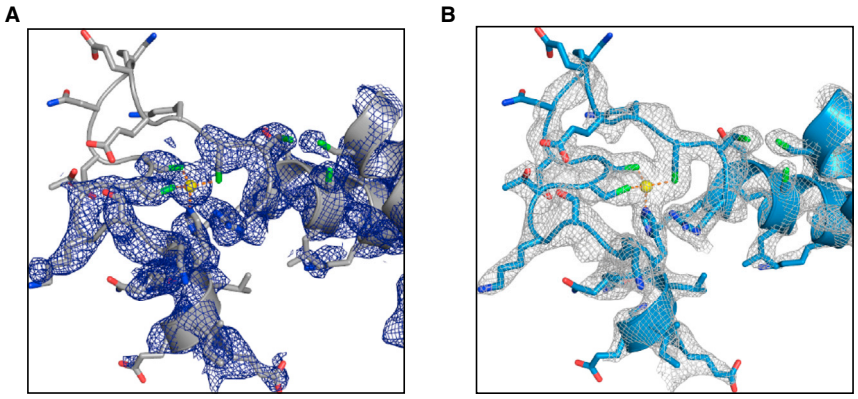

Figure S2. cGAS Experimental and Refined Electron Density Maps, Related to Figure 1

(A and B) Initial experimental density map of the cGAS zinc-coordination region (contoured at 1.5 sigma) following solvent flattening (A) and the cGAS $2F_o$-F_c map (contoured at 2.0 sigma) following model building and completed refinement (B). The zinc ion is displayed as a sphere (yellow) and coordinating amino acids side-chains are connected with dashed lines (orange).

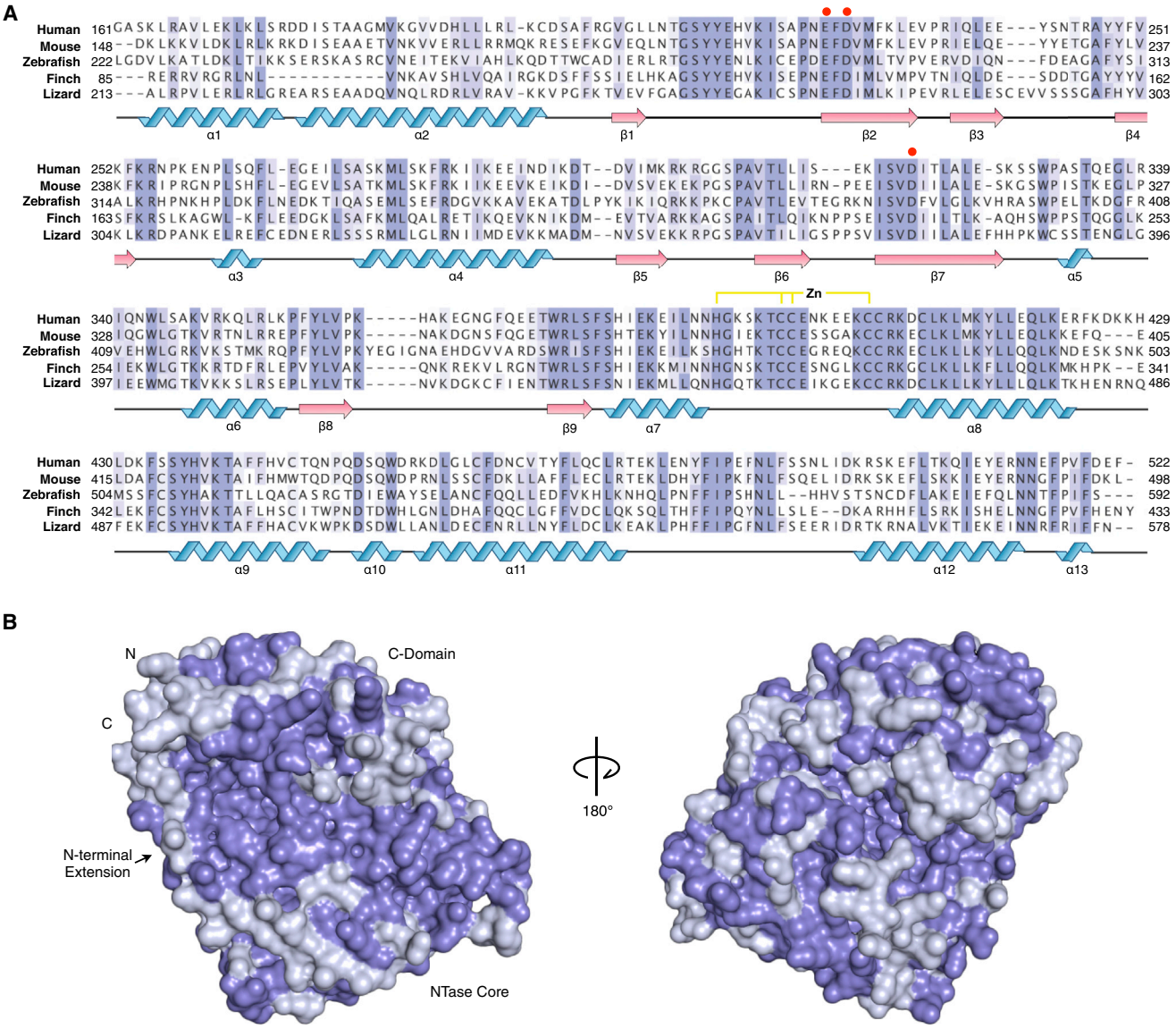

Figure S3. Alignment of Vertebrate cGAS Primary Sequences, Related to Figures 1, 3, and 4

(A) Sequence alignment of representative vertebrate cGAS protein sequences. Amino-acid sequences were aligned using MAFFT (Katoh and Standley, 2013) and colored according to BLOSSUM62 score in Jalview (Waterhouse et al., 2009). Secondary structure from the human cGAS crystal structure is displayed below, active site residues involved in divalent cation coordination are indicated with a red circle, and zinc-coordination residues are indicated between alpha-helices 7 and 8.

(B) Surface representation of the human cGAS structure depicting amino-acid positions conserved between human and mouse (purple) and varying positions (white).

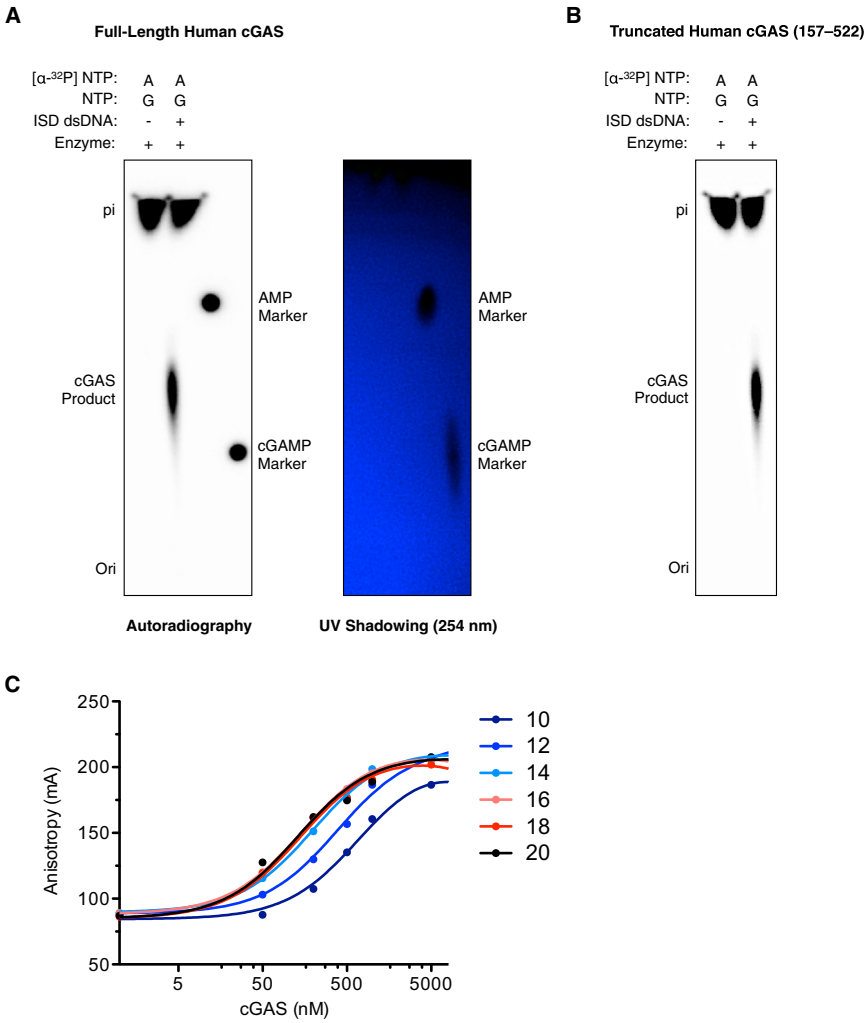

Figure S4. cGAS Cyclic Dinucleotide Synthesis and dsDNA Binding, Related to Figure 2

(A) TLC image displayed in Figure 2B, along with a corresponding image of the UV-shadowed plate. UV-shadowed AMP and cGAMP spots were manually marked with a dot of radiolabeled phosphate.

(B) Cyclic dinucleotide synthesis was reconstituted using identical conditions to those used for full-length cGAS protein (Figure 2), and reaction products were separated by thin-layer chromatography. The cGAS 157–522 fragment retains full catalytic activity and dsDNA-stimulation requirement.

(C) Full-length recombinant cGAS was incubated with dsDNA oligomers of the indicated length (bp) and labeled on the 5′ end of the sense strand with fluorescein. Fluorescence polarization data were measured as in Figure 2, and data were converted to anisotropy to compare relative affinities. Plotted data are representative of individual experiments with all oligomer lengths performed in parallel, and demonstrate that the relative affinity of cGAS for dsDNA increases until ligand length approaches >20 bp.